JACS
JOURNAL OF THE AMERICAN CHEMICAL SOCIETY
Article
pubs.acs.org/JACS
Terms of Use

Surface Effects on Aggregation Kinetics of Amyloidogenic Peptides

Robert Vácha,*[,†] Sara Linse,[‡] and Mikael Lund[§]

[†]National Centre for Biomolecular Research, Faculty of Science and CEITEC - Central European Institute of Technology, Masaryk University, Kamenice 5, 625 00 Brno-Bohunice, Czech Republic

[‡]Division of Biochemistry and Structural Biology, Lund University, Lund, Sweden

[§]Division of Theoretical Chemistry, Lund University, Lund, Sweden

Supporting Information

ABSTRACT: The presence of surfaces influences the fibril formation kinetics of peptides and proteins. We present a systematic study of the aggregation kinetics of amyloidogenic peptides caused by different surfaces using molecular simulations of model peptides and thioflavin T fluorescence experiments. Increasing the monomer−surface attraction affects the nucleation and growth of small oligomers in a nonlinear manner: Weakly attractive surfaces lead to retardation; strongly attractive surfaces lead to acceleration. Further, the same type of surface either accelerates or retards growth, depending on the bulk propensity of the peptide to form fibrils: An attractive surface retards fibril formation of peptides with a high tendency for fibril formation, while the same surface accelerates fibril formation of peptides with a low propensity for fibril formation. The surface effect is thus determined by the relative association propensity of peptides for the surface compared to bulk and by the surface area to protein concentration ratio. This rationalization is in agreement with the measured fibrillar growth of α-synuclein from Parkinson and amyloid β peptide from Alzheimer disease in the presence of surface area introduced in a controlled way in the form of nanoparticles. These findings offer molecular insight into amyloid formation kinetics in complex environments and may be used to tune fibrillation properties in diverse systems.

INTRODUCTION

Amyloid fibril formation is observed in several devastating human diseases, including neurodegenerative conditions such as Alzheimer and Parkinson diseases. In the form of monomers, the proteins involved in these diseases seem to have an extremely low rate of nucleation and self-assembly under normal physiological conditions and concentrations. A major question regards how these diseases start, since once the first amyloid aggregates emerge, there seems to be no return. In vivo, amyloid aggregation occurs in a complex environment including a large number of cosolutes and surfaces. It is therefore essential to identify factors that can initiate the process and to systematically investigate how the aggregation process is enhanced or attenuated by various substances and surfaces. To deepen our understanding of the process and to obtain predictive power it is crucial to relate the observed effects to the molecular properties of the substance or surface as well as the aggregating protein or peptide. Moreover, the increasing use of nanoparticles in technical and biomedical applications[1−3] require systematic studies to understand under which conditions these foreign surfaces catalyze or prevent aggregation.[4,5]

Surfaces have a large impact on the rates of protein aggregation leading to amyloid fibril formation. For example α-synuclein (α-syn) is natively unfolded as a monomer in solution and has a high affinity for various surfaces, including phospholipid membranes.[6−9] Aggregation of α-syn in bulk solution is extremely slow under physiological conditions, but the protein may nucleate at surfaces, leading to amyloid growth along the surface and into solution.[6] α-syn aggregation kinetics starting from monomers has this far only been reported in the presence of binding surfaces such as beads or sample containers of glass or polystyrene, or phospholipid membranes.[7,10−13] However, the surface presented on α-synuclein fibrils seems to catalyze nucleation at mildly acidic pH. Fibril formation is hence observed in the absence of other atractive surfaces, provided a small amount of seed is added to the (monomer) solution.[14] The amyloid β peptide (Aβ42) from Alzheimer disease aggregates slowly at physiological brain fluid concentration (low nM range). However, for this peptide, nucleation in solution is fast enough to form fibrils on a minutes-to-days time scale in pure monomer solutions exceeding ca. 100 nM peptide concentration in sample containers with a nonbinding PEG-ylated surface that has no measurable affinity for Aβ.[15,16] Also this protein is affected by various surfaces. Fibrils of the same peptide can represent surfaces that speed up the aggregation process in an autocatalytic manner.[16−18] The process is also sensitive to foreign surfaces such as cuvettes, test tubes, or nanoparticles and may be accelerated[4,19] or

Received: June 5, 2014
Published: July 28, 2014

   dx.doi.org/10.1021/ja505502e | J. Am. Chem. Soc. 2014, 136, 11776−11782

retarded[19−23] depending on both the surface chemistry and the physicochemical properties of the protein and its bulk aggregation behavior. The surface area to protein concentration ratio plays a critical role and can lead to either catalysis or retardation.[19]

While aggregation rates of proteins correlate with the stability toward unfolding of the respective monomeric protein,[24,25] the same property seems to govern the effect of surfaces. In a series on monellin mutants, the surface presented on polymeric nanoparticles was found to catalyze the fibril formation of relatively stable variants with slower aggregation in bulk, while the same surface retards the fibril formation of relatively unstable variants with faster aggregation in bulk.[20]

To summarize, the effects of surfaces on aggregation kinetics are profound and the coupling to molecular driving forces is poorly understood. The present work sets out to rationalize current observations using a simplified molecular model where intermolecular interactions and kinetics can be varied in a controlled fashion. We have previously found that Monte Carlo simulations with simplified potentials offer an insightful way to identify general factors affecting the fibril formation process.[26,27] Here, molecular detail is extracted from dynamic Monte Carlo simulations of amyloid growth in bulk and in the presence of surfaces with varying attraction potential, coupled with fluorescence spectroscopy measurements in the presence of nanoparticles with varying ratios of surface area to bulk protein and salt concentration.

METHODS

Dynamic Monte Carlo Simulation. The amyloidogenic peptides were modeled as patchy spherocylinders (PSC),[26] i.e. cylinders with hemispherical caps at both ends and with an attractive stripe on one side. As in a previous study on the nucleation and growth of an amyloid-like structure,[28] the model includes two states: α, corresponding to the folded solution structure, and β, corresponding to the β-sheet structure found in amyloids. In brief, the size of the PSC was 1 × 6 nm^2 with an attractive stripe of 90° for the α-state and 180° for the β-state. The PSC dimensions correspond to roughly 30 amino acids, a typical value seen in β-sheet strands in amyloid fibril structures. It is unlikely that the thickness has any significant effect, as it only determines the spacing in the fibrils. The effective implicit solvent interactions between the attractive stripes are −8.4 k_BT and −21 k_BT for the α and β state, respectively. These effective stripe interactions include hydrophobic interactions, hydrogen bonds, salt-bridges, etc. The β-state has a chirality of 10°, and the transition free energy from $\alpha \rightarrow \beta$ is 15 k_BT. In each simulation step, the intrinsic transition probability was 1.6 × 10^{-3}.

We used the dynamic Monte Carlo (DMC)[29−31] simulation method—shown to converge to Brownian dynamics[32]—where configurations are sampled in the *NVT* ensemble (i.e., with constant volume, temperature, and number of molecules) using a prismatic, slit geometry, where we varied the protein interaction strength of the flat, facing surfaces; see Figure 1. The displacement parameters of translational and rotational moves were matched to experimental translational (D_T) and rotational (D_R) diffusion constants of the Aβ amyloid forming peptide with D_T = 0.15 nm^2 ns^{-1} and D_R = 0.08 ns^{-1} at 300 K.[33] In contrast to conventional Metropolis Monte Carlo, displacements in DMC are small enough to ensure physical moves and the maximum PSC displacement and rotation per step were 0.212 nm and 7.5°, respectively. Together with the diffusion constants above, these define the time scale of a simulation step—where on average all particles have been updated—to 0.02 ns. For each simulated condition, three to six separate runs were conducted with different random initial configurations and the obtained growth profiles were averaged over all runs.

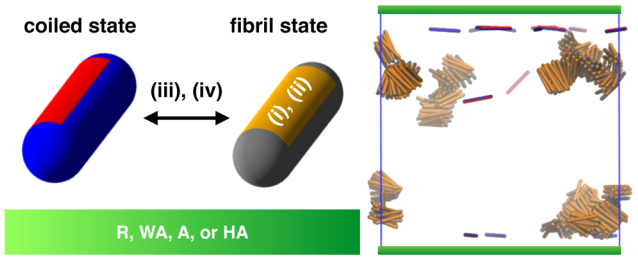

Figure 1. (Left) Two-state peptide model used in dynamic Monte Carlo simulations in the presence of planar surfaces (green). Kinetic and thermodynamic properties are described by the parameters (i) → (iv), discussed in the section "Surface Effect for Peptide Mutants", as well as through a surface attraction strength, K (Table 1). (Right) Representative snapshot from our simulation where orange/gray are particles in the fibril state, while blue/red particles are in the random coil state.

Unless otherwise stated, the system was composed of 200−800 PSC peptides, and the slit dimensions were 50 × 50 × 50 nm^3, corresponding to the concentration range 3−11 mM. The interaction with slit walls was calculated using the spherocylinder line segment projected onto the wall in the direction of its patch and truncation of the projected segment by a cutoff. The resulting interaction profiles between PSC and the wall can be found in Figure 2. The interaction

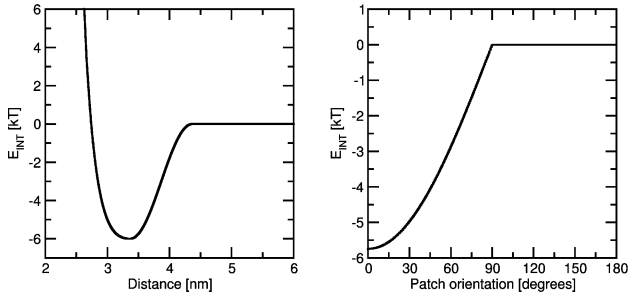

Figure 2. Interaction energy between a weakly attractive surface (WA) and the α state of the peptide. The left figure depicts the distance dependence of the interaction when PSC is parallel to the wall oriented with its patch toward the wall. The right figure displays the orientation dependence of the interaction when PSC is parallel to the wall in distance close to the interaction minimum.

strength between different species was calculated using Berthelot's rule[34] as in our previous study.[28] The monomer−surface binding constant, K, is defined as

$$1/K \approx \rho \int_c^\infty (\exp[-w(r)/k_BT] - 1)\, dr \quad (1)$$

where $w(r)$ is the angularly averaged potential of mean force between a monomer and the surface, k_BT is the thermal energy, c is the contact distance where w = 0, and ρ = 21 Å^2 is the maximum monomer coverage in the Langmuir adsorption model.

Kinetic Experiments. *Materials.* The Aβ42(M1−42) peptide (MDAEFRHDSGYEVHHQKLVFFAEDVGSNKGAIIGLMVGGVVIA), here called Aβ42, was expressed in *Escherichia coli* from a synthetic gene and purified as described by Walsh et al.[35] with the exception that size exclusion with spin filters was replaced by gel filtration. In short, the purification procedure involved sonication of *E. coli* cells, dissolution of inclusion bodies in 8 M urea, ion exchange in batch mode on DEAE cellulose resin, lyophilization, and gel filtration on a 3.4 cm wide × 200 cm tall gel filtration column at 4 °C. The purified peptide was frozen as identical 3 mL aliquots and lyophilized. All chemicals were of analytical grade. Human α-synuclein was expressed in *E. coli* from a Pet-plasmid (kind gift from H. Lashuel, Lausanne) and purified from the soluble fraction using sonication,

dx.doi.org/10.1021/ja505502e | J. Am. Chem. Soc. 2014, 136, 11776−11782

boiling, and ion exchange chromatography as described[7] and stored as frozen aliquots. Nanoparticles: Plain polystyrene nanoparticles of 23 nm diamater, polystyrene nanoparticles of 26 nm diameter with COOH-groups, and polystyrene nanoparticles of 57 nm diamater with NH_2-groups were obtained from Bangs laboratories (Fishers, Indiana) and were dialyzed against the experimental buffers with daily exchange for 2 weeks before use.

Preparation of Samples for Experiments. For kinetic experiments, aliquots of purified Aβ42 were dissolved in 6 M guanidinium chloride (GuHCl), and the monomer was isolated by gel filtration on a 1 cm wide × 30 cm tall Superdex 75 column in 20 mM sodium phosphate buffer, pH 8, with 0.2 mM EDTA and 0.02% NaN_3. The center of the monomer peak was collected on ice and lyophilized. The sample was again dissolved in 6 M GuHCl, and the monomer was isolated by gel filtration on a Superdex 75 column in 20 mM sodium phosphate buffer, pH 8, with 0.2 mM EDTA and 0.02% NaN_3. The gel filtration steps remove traces of pre-existent aggregates and exchanges the buffer to the one used in the fibril formation experiments. The peptide concentration was determined from the absorbance of the integrated peak area using ϵ_{280} = 1400 L mol^{-1} cm^{-1} as calibrated using quantitative amino acid analysis. The monomer generated in this way was diluted with buffer to 12 μM. Nanoparticles were prepared as a dilution series at two times the desired final concentration. ThioflavinT (ThT) was added from a 1.2 mM stock to a final concentration of 6 μM, as chosen in a range that produces a fluorescence signal that is linearly related to the fibril concentration.[16] These solutions were then mixed 1:1 with Aβ42 to obtain a final concentration of 6 μM Aβ42 and no or between 0.002 and 0.11 g/L nanoparticles. All samples were prepared in low-bind Eppendorff tubes (Axygen, California, USA) on ice using careful pipetting to avoid introduction of air bubbles. Each sample was then pipetted into multiple wells of a 96 well half-area plate of black nonbinding plates with a clear bottom (Corning 3881, Massachusetts, USA), 100 μL per well.

The α-synuclein monomer was isolated by gel filtration on a 1 cm wide × 30 cm tall Superdex 75 column in 10 mM Mes/NaOH pH 5.5. The center of the monomer peak was collected. The protein concentration was determined from the absorbance of the integrated peak area using ϵ_{280} = 5800 L mol^{-1} cm^{-1}. Samples were prepared by a 1:1 mixing of protein and nanoparticle stocks to obtain a final concentration of 20 μM α-synuclein and 10 μM ThT without or with polystyrene nanoparticles (diameter 23 nm) ranging from 0.001 to 0.5 g/L in 2-fold increments. Each sample was pipetted into multiple wells of a 96 well half-area plate of black nonbinding plates with a clear bottom (Corning 3881, Massachusetts, USA).

Kinetic Assays. Assays were initiated by placing the 96-well plate at 37 °C under quiescent conditions in a plate reader (Fluostar Omega or Optima, BMGLabtech, Offenburg, Germany). The ThT fluorescence was measured through the bottom of the plate every 60 s using a 440 nm excitation filter and a 480 nm emission filter. The ThT fluorescence was followed for four to six repeats of each sample, and the whole setup was repeated twice in separate plates.

RESULTS AND DISCUSSION

Effect of Wall Binding Strength. We have simulated amyloid aggregate nucleation and growth in the presence of hard, planar surfaces to which monomers are repelled or attracted according to the binding constants listed in Table 1.

Table 1. Peptide Binding Constants to Four Different Planar Surfaces

surface type		$K/\mu M^{-1}$
repulsive	R	~0
weakly attractive	WA	0.0017
attractive	A	0.075
highly attractive	HA	0.16

Figure 3 shows oligomer growth profiles at different peptide concentrations for each surface type accompanied by representative snapshots. There is a dramatic difference between the surface effects on fibril formation. A *weakly* attractive (WA) surface decreases the nucleation rate compared to a purely repulsive surface (R). This is because the former surface adsorbs monomers and thus decreases the bulk concentration. At the same time there is no appreciable surface nucleation, leading to overall growth retardation. Nuclei are formed in bulk solution, and the final oligomer structure is the same as in pure bulk. Note that fibrils were identified as tetramers and larger oligomers, since the tetramer is the minimum nucleation size of the employed model in bulk growth of amyloid-like structures.[28] Changing the definition of fibrils to hexamers did not change the observed trends.

The opposite behavior is observed for *highly* attractive (HA) surfaces, where nuclei are formed at the interface and fibril formation is faster than at the repulsive (R) surface for each simulated concentration. The attractive surface (A) lies between the WA and HA surfaces and leads to similar overall kinetics as the repulsive (R) surface. However, the systems R and A are different in location and morphology of fibrils; see Figure 3. The surface oligomers (systems A and HA) have different conformations compared to those formed in solution (in system R). While double layer ribbons were formed in solution, surface fibrils were composed of a monolayer ribbon with the hydrophobic part oriented toward the surface. Such surface fibrils are less rigid and readily break due to competition with the attractive surface.

The above results are valid over the range of tested peptide concentrations, 3−11 mM, and the observed growth acceleration or retardation depends solely on the surface binding strength. This is shown in Figure 4, right, via half times plotted as a function of the surface affinity.

Effect of Surface/Bulk Ratio. The influence of the surface/bulk ratio on oligomer growth was studied by additional simulations with a fixed surface area (500 nm^2) while increasing the bulk volume from 1.25 × 10^5 to 7.5 × 10^5 nm^3. The PSC peptide concentration in all systems was kept fixed at 2.66 mM. Figure 4, right, shows that the surface effect is decreased by increasing the bulk volume, and as expected, all lines eventually converge to the bulk limit. Indeed, bulk expansion for the WA surface leads to bulk nucleation with a half-time similar to that of the R surface. Still, all nuclei were formed at the highly attractive (HA) surface even for the largest bulk volume, and the observed growth retardation with increasing volume is thus due to the increased diffusion time to reach the surface. Nevertheless, we expect that an even further increase of the bulk would eventually lead to bulk nucleation and growth, similar to the system with a repulsive surface. The full growth curves are displayed in the Supporting Information.

Surface Effect for Peptide Mutants. Is fibrillar retardation an intrinsic property of the WA surface? To test this, we studied different peptide mutants and compared the growth to the repulsive (R) surface. The advantage of the simplified simulation model is that molecular properties can be mutated in a controlled fashion by varying the following parameters (see Figure 1):

(i) *monomer−monomer interaction strength* corresponding to additional hydrogen bonds, salt bridges, coulomb

dx.doi.org/10.1021/ja505502e | J. Am. Chem. Soc. 2014, 136, 11776−11782

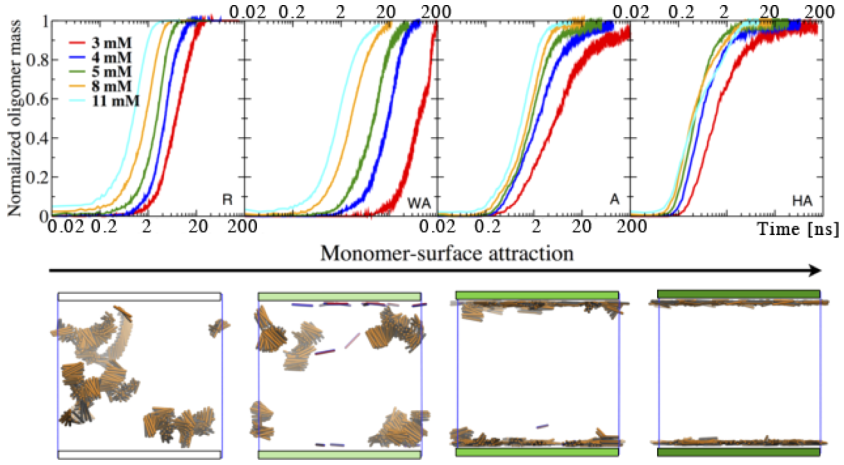

Figure 3. (Top) Oligomer growth profiles in the presence of planar surfaces with increasing binding strengths (see Table 1) and monomer concentration (colored lines). Each profile represents an average from at least three independent simulations. (Bottom) Corresponding snapshots at an initial monomer concentration of 5.3 mM.

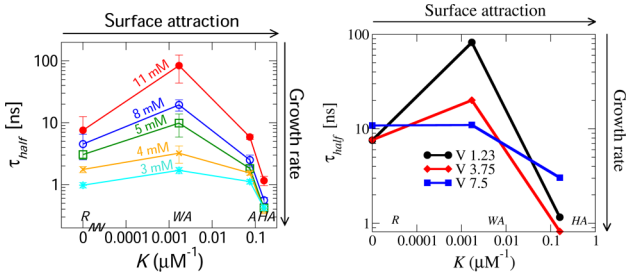

Figure 4. (Left) Half times, τ_{half}, of the fibril formation in systems with varying monomer affinities for the surface. (Right) τ_{half} for systems with increasing bulk/surface ratio as a function of surface binding strength. Increased bulk volume is depicted by black circles (1.25×10^5 nm^3), red diamonds (3.75×10^5 nm^3), and blue squares (7.5×10^5 nm^3). The half times represent the time where 50% of the monomers have formed fibrils averaged over three independent simulation runs, and the error bars display the standard deviation.

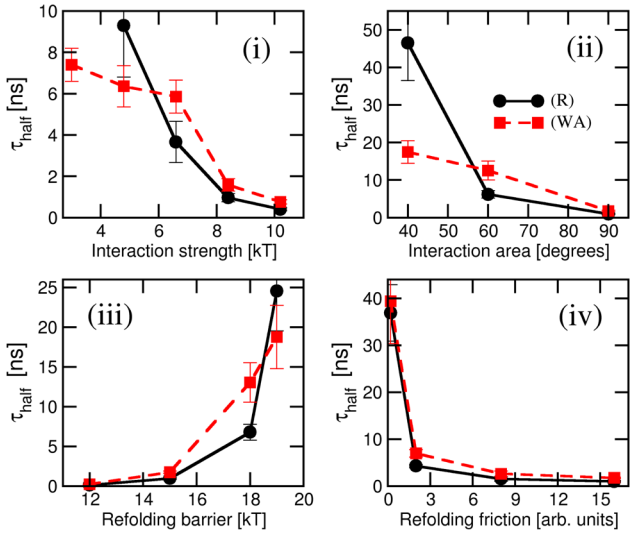

Figure 5. Half times of fibrillar growth of peptide mutants at the repulsive (R) and at the weakly attractive (WA) surfaces. The mutation types are peptide−peptide attraction (top left), width of attractive patch (top, right), $\alpha \rightarrow \beta$ transition barrier (bottom, left), and folding probability/friction (bottom, right).

interaction, etc. within the same monomer−monomer attractive area;

(ii) *patch size* corresponding to added hydrophobic residues or other interactions that result in the same interaction density, but larger attractive area on PSC;

(iii) *the free energy of the fibrillar conformation* corresponding to mutations that affect the free energy difference between solution and the fibrillar state (refolding free energy difference); and

(iv) *probability of attempts to switch from solution to the fibrillar state* corresponding to modified refolding kinetics (internal friction to refold).

The half times of fibrillar growth shown in Figure 5 show that retardation is not an intrinsic property of the WA surface, which can both retard or accelerate the fibril formation depending on the particular peptide. For mutants (i), (ii), and (iii), there is a clear cross section of lines with circles and squares representing a point where the growth is roughly the same for the WA and the R surfaces. This point is not clear in the case of (iv) mutants, but from growth curves (see SI) there may be one for even larger mutations. Interestingly, fibril formation of less amyloidogenic mutants, i.e. with higher intrinsic stability, is accelerated by the WA surface, while the growth of more fibril prone mutants is retarded by the WA surface compared to the R surface.

Experiment: Effect of Nanoparticles on α-Synuclein Aggregation. We will now validate the simulation results by experimentally investigating the effect of the surface/bulk ratio for a system with attractive peptide−surface interactions. The aggregation of 20 μM α-synuclein into amyloid fibrils was studied by ThT fluorescence in the absence and presence of the increasing concentration of 23 nm diameter polystyrene nanoparticles in 10 mM MES buffer, pH 5.5. In the absence of nanoparticles, no increase in ThT fluorescence is observed, implying that the protein remains monomeric in solution over the time course of the experiment (215 h). In contrast, the data obtained in the presence of nanoparticles have a sigmoidal-like appearance with a lag phase, a growth phase, and an equilibrium plateau at 0.125 and 0.25 g/L nanoparticles, with some variation in shape at 0.06 g/L (Figure 6). The process is clearly accelerated by the presence of polystyrene nanoparticles

dx.doi.org/10.1021/ja505502e | J. Am. Chem. Soc. 2014, 136, 11776−11782

in a reproducible manner depending on the surface area presented.

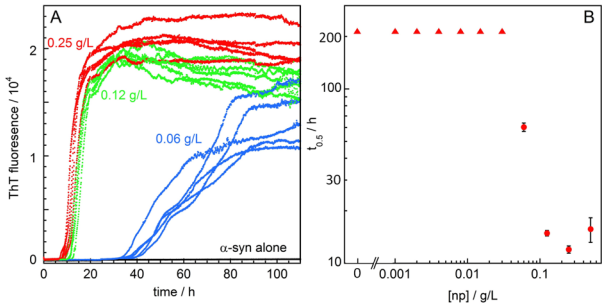

Figure 6. Aggregation kinetics for 20 μM α-synuclein in 10 mM MES/NaOH pH 5.5 in the absence and presence of 23 nm polystyrene nanoparticles. (A) ThT fluorescence as a function of time with no (black), 0.06 g/L (blue), 0.12 g/L (green), or 0.25 g/L (red) nanoparticles. The first 110 h are shown. (B) Half time (average and standard deviation) for fibrillar growth as a function of nanoparticle concentration. The triangles indicate that no aggregation is observed over 215 h in samples with 0.03 g/L or less nanoparticles.

The nanoparticle concentrations that lead to sigmoidal aggregation curves within the time frame of the experiment (0.06, 0.125, 0.25, and 0.5 g/L) correspond to total surface areas of 16, 32, and 65 and 130 m^2/L, respectively, assuming perfect spheres. This means that the 135, 270, 540, or 1080 $Å^2$ surface area is available per protein molecule in a 20 μM solution. At least in the three lowest concentrations there is less surface than can bind all protein molecules in one densely packed layer, whereas 1080 $Å^2$ is close to the cross section area as expected for a globular protein of 14 kDa.

At pH 5.5 α-synuclein is negatively charged ($\approx -4e$) and lack of self-association in bulk is likely caused by electrostatic repulsion. In our simulation model this corresponds to a very weak peptide–peptide interaction strength, cf. Figure 5, top left. As forecasted by the model, a strong, nonelectrostatic attraction between the polystyrene surface and peptide leads to fibrillar growth acceleration upon increasing the surface/bulk ratio (Figure 4, left).

Experiment: Effect of Nanoparticles on Aβ42 Aggregation. In this section we investigate the effect of peptide–surface interaction strength by introducing charged surfaces and varying the electrostatic screening using salt. The aggregation of 6 μM Aβ42 into amyloid fibrils was studied by ThT fluorescence in the absence and presence of an increasing concentration of nanoparticles at low salt, as well as at 50 and 300 mM NaCl in 20 mM sodium phosphate buffer, 0.2 mM ETDA, pH 8.0. All curves are sigmoidal-like with a lag phase, a growth phase, and an equilibrium plateau, with some variation in shape. The time at which half the monomers are consumed, i.e. the time at which half the final ThT intensity over the initial baseline is reached, τ_{half}, is extracted from each curve and plotted in Figure 7. Clearly, the process is affected by the presence of polystyrene nanoparticles in a manner depending on the surface charge and concentration. Negatively charged surfaces cause a retardation of aggregation. This is most pronounced when no salt is added, in which case τ_{half} increases with nanoparticle concentration up to around 0.022 g/L where τ_{half} is doubled. At higher nanoparticle concentration (larger surface area), τ_{half} is again decreasing and at 0.11 g/L the value is the same as that in the absence of nanoparticles. At an even

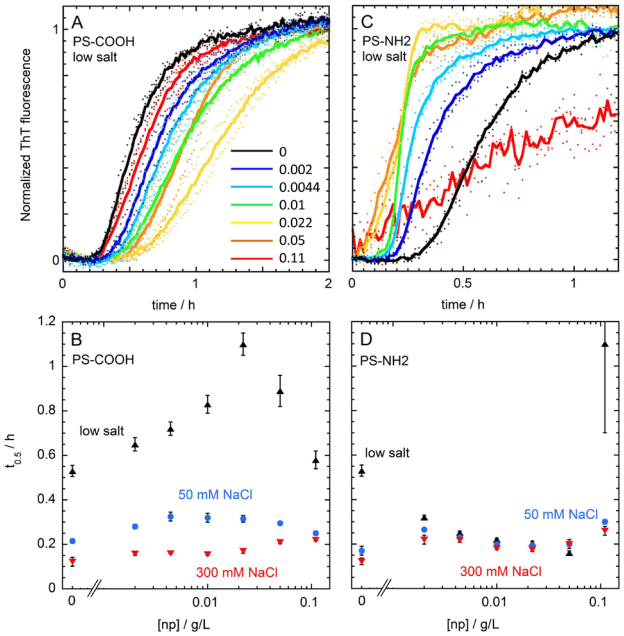

Figure 7. Aggregation kinetics for 6 μM Aβ42 in 20 mM sodium phosphate, 0.2 mM EDTA, pH 8.0 in the absence and presence of nanoparticles. (A and C) ThT fluorescence as a function of time with no (black), 0.002 (blue), 0.0044 (light blue), 0.01 (green), 0.022 (yellow), 0.05 (orange), or 0.11 (red) g/L polystyrene nanoparticles of 26 nm diameter with COOH-groups (A) or of 57 nm with NH_2-groups (C). The first 2 and 1.2 h are shown, respectively. (B and D) Half times of fibrillar growth as a function of the concentration of nanoparticles (B: anionic, D: cationic) at low, 50, and 300 mM NaCl.

higher nanoparticle concentration, the ThT signal is distorted and measurements become unreliable. In the presence of positively charged nanoparticles we observe the opposite trend with catalysis up to 0.05 g/L, while the next concentration (0.11 g/L) cause retardation. The turnover occurs between 0.05 and 0.11 g/L nanoparticles, presenting a surface of 2–4 m^2/L assuming perfect spheres of 57 nm diameter, equivalent to 500–1000 $Å^2$ per Aβ42 peptide. Thus, the process is increasingly catalyzed until the total surface area is approximately that required to bind all peptides, in agreement with a previous report.[19] The interaction between Aβ42 and the surfaces is modulated by the addition of salt which for both negative and positive surfaces attenuates the effect. At 300 mM NaCl, the addition of negatively charged nanoparticles leads to an earlier onset of aggregation (shortened lag phase) but the overall aggregation profile is less steep, leading to a largely similar τ_{half}.

At pH 8, Aβ42 is negatively charged ($\approx -3e$), and for a cationic surface, the strong attractive electrostatic contribution to the peptide–surface interaction enhances growth; less so when screening salt is added. This can be explained by an enhanced surface nucleation due to a higher surface concentration. As more surface is added, the local concentration eventually decreases (due to dilution), leading to growth retardation. This was observed also for α-synuclein at the largest concentration of the nanoparticles. The effect of salt addition is 2-fold: both the peptide–peptide repulsion and peptide–surface interactions are screened. While salt screening of the peptide–surface interaction decelerates growth, it also reduces the peptide–peptide repulsion, leading to acceleration, and the final result is thus a mix of the two effects. This

dx.doi.org/10.1021/ja505502e | J. Am. Chem. Soc. 2014, 136, 11776–11782

qualitative analysis is fully consistent with the simulation model; see Figure 5, top left. Quantitative agreement between simulations and experiment is not to be expected due to the simplicity of the model and the fact that surface fibrils can have different morphology than in the bulk and can therefore result in a different amount of the ThT signal.

In the case of an anionic surface, a small amount of nanoparticles retards growth at low salt concentrations. This is likely due to a *weak* surface adsorption (caused by non-electrostatic forces) which—as shown by the simulations, see Figure 4—retards fibrillation by decreasing the bulk concentration. At even higher nanoparticle concentrations bulk kinetics is restored. The turnover occurs around 0.022 g/L nanoparticles, representing a surface of ca. 4 m^2/L assuming perfect spheres, equivalent to ca. 1000 $Å^2$ per Aβ42 peptide. Thus, opposite to the cationic nanoparticle, the process in the presence of anionic nanoparticles is increasingly retarded until the total surface area is approximately that required to bind all peptides. Upon salt addition, repulsive electrostatic peptide−peptide and peptide−surface interactions are weakend, leading to faster kinetics over the entire range of nanoparticle concentrations as also observed in the simulations when increasing the attractive interaction strength (Figure 5, top left).

Rationalization of Existing Studies. In summary, both simulations and experiments show that surfaces can cause retardation or acceleration of the kinetics of aggregate growth. Further, one surface can lead to both effects, depending on the specific peptide and surface properties, as well as on the surface area to protein concentration ratio. This can be rationalized by competition between surface and bulk for the nucleation and growth processes. When aggregation at an adsorbing surface is slower than in bulk, the overall growth in the system is retarded due to monomer depletion in the bulk. If, however, surface aggregation is faster than in bulk, the overall growth in the system can be accelerated. Our finding that some surfaces enhance Aβ peptide aggregation while others inhibit or considerably slow down fibril formation is in agreement with recent observations by dual polarization interferometry.[36] Further, lipid vesicles were reported to accelerate or retard the fibrillar growth of different peptides, which is also in accord with our data.[37−41]

The present findings clarify a range of recent experimental studies on amyloid growth of peptide mutants in the presence of nanoparticles which show both retardation and acceleration. Particularly, for mutants with high intrinsic stability and low intrinsic aggregation the rate of amyloid formation is accelerated by nanoparticles, while for mutants with a low intrinsic stability and high intrinsic aggregation rate amyloid formation is retarded by nanoparticles.[20] An advantage of a simplified model is that we can modify the parameters of mutants separately. Experimentally, a single mutation would typically influence more parameters of our model, yet all parameters follow the same trend, showing that our results are robust and general.

Electron microscopy revealed the formation of amyloid fibrils detached from the nanoparticle surface.[4] Moreover, the half ribbon conformation obtained for the surface fibrils in simulations agrees with spectroscopic and AFM experiments as well as with coarse-grained and all-atom simulations of peptides at hydrophobic surfaces like C18 or graphite, observed to promote amyloid fibril formation.[36,42−46] Ribbons were also observed for the cationic amyloidogenic peptide KIGAKI on a phospholipid membrane.[47]

The current predictions on kinetics are based on a generic, coarse grained model, rigorously evaluated using statistical mechanics. The findings are hence likely to be general. Despite no significant secondary nucleation events (surface seeding or fibril breakage) in our simulation, the surface is likely to have the same effect on kinetics involving secondary nucleation pathways, since our findings are based on the change of local concentration. Yet there could be deviations and more complex behavior due to higher order kinetics and the relative influence of the surfaces on different microscopic steps in the process.[48] Further, the perfectly flat homogeneous surfaces in the simulations allow for relatively fast interfacial diffusion (same as in bulk). Surface roughness can slow diffusion and delay nucleation, and even highly attractive surfaces may thus lead to retardation of fibrillar growth.[49] Lastly, local inhomogeneities can result in local nucleation and alter the overall effect of the surface.[50] Despite these approximations, the present phenomenological model is in very good agreement with experimental data and provides a molecular picture for the underlying mechanisms.

■ CONCLUSION

We have investigated surfaces with different peptide binding strengths and their influence on fibril formation. The observed effect is nonlinear. While weakly attractive surfaces lead to retardation of nucleation and growth, strongly attractive surfaces lead to acceleration of the fibril formation. The molecular rationalization lies in a competition between two processes: surface and bulk nucleation, which lead to the observed growth. The surface effect is dependent on the intrinsic aggregation characteristics of peptides and proteins: A surface with weak monomer attraction *retards* the fibril formation of peptides with a high tendency for fibril formation, while the same surface *accelerates* the fibril formation of peptides with a low propensity for fibril formation. The presented study rationalizes current and previous experimental data for a number of different systems, and together with the fact that we use a generic, coarse grained model within a rigorous statistical mechanical framework, we expect the proposed molecular mechanism to be general and broadly applicable.

■ ASSOCIATED CONTENT

Ⓢ Supporting Information

This information contains all experimental and simulation growth profiles (Figures S1−S3). This material is available free of charge via the Internet at http://pubs.acs.org.

■ AUTHOR INFORMATION

Corresponding Author

robertvacha@gmail.com,robert.vacha@mail.muni.cz

Notes

The authors declare no competing financial interest.

■ ACKNOWLEDGMENTS

This work was supported by the Swedish Research Council and its Linneaus Centre OMM (organizing molecular matter); the Swedish Foundation for Strategic Research; eSSENCE, nanometer structure consortium, and LUNARC at Lund University; the Czech Science Foundation (Grant 14-12598S); the EU seventh Framework (Contract No. 286154 - SYLICA); the

European Regional Development Fund (CZ.1.05/1.1.00/02.0068 CEITEC); and MetaCentrum LM2010005.

REFERENCES

(1) Tang, F.; Li, L.; Chen, D. *Adv. Mater.* **2012**, *24*, 1504−1534.
(2) Zahmakran, M.; Özkar, S. *Nanoscale* **2011**, *3*, 3462−3481.
(3) Spyratou, E.; Makropoulou, M.; Mourelatou, E.; Demetzos, C. *Cancer Letters* **2012**, *327*, 111−122.
(4) Linse, S.; Cabaleiro-Lago, C.; Xue, W.-F.; Lynch, I.; Lindman, S.; Thulin, E.; Radford, S. E.; Dawson, K. A. *Proc. Natl. Acad. Sci. U. S. A.* **2007**, *104*, 8691−8696.
(5) Lynch, I.; Dawson, K. A.; Linse, S. *Sci. STKE* **2006**, *2006*, pe14.
(6) Rabe, M.; Soragni, A.; Reynolds, N. P.; Verdes, D.; Liverani, E.; Riek, R.; Seeger, S. *ACS Chem. Neurosci.* **2013**, *4*, 408−17.
(7) Grey, M.; Linse, S.; Nilsson, H.; Brundin, P.; Sparr, E. *J. Parkinsons Dis.* **2011**, *1*, 359−371.
(8) Pandey, A. P.; Haque, F.; Rochet, J.-C.; Hovis, J. S. *Biophys. J.* **2009**, *96*, 540−51.
(9) Jo, E.; McLaurin, J.; Yip, C. M.; St. George-Hyslop, P.; Fraser, P. E. *J. Biol. Chem.* **2000**, *275*, 34328−34.
(10) Butterfield, S. M.; Lashuel, H. a. *Angew. Chem., Int. Ed.* **2010**, *49*, 5628−54.
(11) Relini, A.; Cavalleri, O.; Rolandi, R.; Gliozzi, A. *Chem. Phys. Lipids* **2009**, *158*, 1−9.
(12) Giehm, L.; Lorenzen, N.; Otzen, D. E. *Methods (San Diego, Calif.)* **2011**, *53*, 295−305.
(13) Pronchik, J.; He, X.; Giurleo, J. T.; Talaga, D. S. *J. Am. Chem. Soc.* **2010**, *132*, 9797−803.
(14) Buell, A. K.; Galvagnion, C.; Gaspar, R.; Sparr, E.; Vendruscolo, M.; Knowles, T. P. J.; Linse, S.; Dobson, C. M. *Proc. Natl. Acad. Sci. U.S.A.* **2014**, DOI: 10.1073/pnas.1315346111.
(15) Hellstrand, E.; Boland, B.; Walsh, D. M.; Linse, S. *ACS Chem. Neurosci.* **2010**, *1*, 13−18.
(16) Cohen, S. I. A.; Linse, S.; Luheshi, L. M.; Hellstrand, E.; White, D. A.; Rajah, L.; Otzen, D. E.; Vendruscolo, M.; Dobson, C. M.; Knowles, T. P. J. *Proc. Natl. Acad. Sci. U.S.A.* **2013**, 9758−9763.
(17) Arosio, P.; Cukalevski, R.; Frohm, B.; Knowles, T. P. J.; Linse, S. *J. Am. Chem. Soc.* **2014**, *136*, 219−225.
(18) Meisl, G.; Yang, X.; Hellstrand, E.; Frohm, B.; Kirkegaard, J. B.; Cohen, S. I. A.; Dobson, C. M.; Linse, S.; Knowles, T. P. J. *Proc. Natl. Acad. Sci. U.S.A.* **2014**, *111*, 9384−9389.
(19) Cabaleiro-Lago, C.; Quinlan-Pluck, F.; Lynch, I.; Dawson, K. A.; Linse, S. *ACS Chem. Neurosci.* **2010**, *1*, 279−87.
(20) Cabaleiro-Lago, C.; Szczepankiewicz, O.; Linse, S. *Langmuir* **2012**, *28*, 1852−1857.
(21) Cabaleiro-Lago, C.; Quinlan-Pluck, F.; Lynch, I.; Lindman, S.; Minogue, A. M.; Thulin, E.; Walsh, D. M.; Dawson, K. A.; Linse, S. *J. Am. Chem. Soc.* **2008**, *130*, 15437−43.
(22) Cabaleiro-Lago, C.; Lynch, I.; Dawson, K. A.; Linse, S. *Langmuir* **2010**, *26*, 3453−61.
(23) Hellstrand, E.; Sparr, E.; Linse, S. *Biophys. J.* **2010**, *98*, 2206−14.
(24) Booth, D. R.; Sunde, M.; Bellotti, V.; Robinson, C. V.; Hutchinson, W. L.; Fraser, P. E.; Hawkins, P. N.; Dobson, C. M.; Radford, S. E.; Blake, C. C.; Pepys, M. B. *Nature* **1997**, *385*, 787−93.
(25) Szczepankiewicz, O.; Cabaleiro-Lago, C.; Tartaglia, G. G.; Vendruscolo, M.; Hunter, T.; Hunter, G. J.; Nilsson, H.; Thulin, E.; Linse, S. *Mol. BioSyst.* **2011**, *7*, 521−32.
(26) Vácha, R.; Frenkel, D. *Biophys. J.* **2011**, *101*, 1432−1439.
(27) Linse, B.; Linse, S. *Mol. BioSyst.* **2011**, *7*, 2296−2303.
(28) Bieler, N. S.; Knowles, T. P. J.; Frenkel, D.; Vácha, R. *PLoS Comput. Biol.* **2012**, *8*, e1002692.
(29) Kikuchi, K.; Yoshida, M.; Maekawa, T.; Watanabe, H. *Chem. Phys. Lett.* **1991**, *185*, 335−338.
(30) Fichthorn, K. A.; Weinberg, W. H. *J. Chem. Phys.* **1991**, *95*, 1090−1096.
(31) Sanz, E.; Marenduzzo, D. *J. Chem. Phys.* **2010**, *132*, 194102.
(32) Jabbari-Farouji, S.; Trizac, E. *J. Chem. Phys.* **2012**, *137*, 054107.
(33) Bora, R. P.; Prabhakar, R. *J. Chem. Phys.* **2009**, *131*, 155103.
(34) Berthelot, D.; Van der Waals; Leduc, A. *Comptes Rendus Hebdomadaires des Seances de l'Academie des Sciences* **1898**, 1703−1706.
(35) Walsh, D. M.; Thulin, E.; Minogue, A. M.; Gustavsson, N.; Pang, E.; Teplow, D. B.; Linse, S. *FEBS J.* **2009**, *276*, 1266−81.
(36) Zhai, J.; Lee, T.-H.; Small, D. H.; Aguilar, M.-I. *Biochemistry* **2012**, *51*, 1070−8.
(37) Knight, J. D.; Miranker, A. D. *J. Mol. Biol.* **2004**, *341*, 1175−1187.
(38) Friedman, R.; Pellarin, R.; Caflisch, A. *J. Mol. Biol.* **2009**, *387*, 407−415.
(39) Volles, M. J.; Lee, S.-J.; Rochet, J.-C.; Shtilerman, M. D.; Ding, T. T.; Kessler, J. C.; Lansbury, P. T. *Biochemistry* **2001**, *40*, 7812−7819.
(40) Sharp, J. S.; Forrest, J. A.; Jones, R. A. L. *Biochemistry* **2002**, *41*, 15810−15819.
(41) Pellarin, R.; Caflisch, A. *J. Mol. Biol.* **2006**, *360*, 882−892.
(42) Losic, D.; Martin, L. L.; Aguilar, M.-I.; Small, D. H. *Biopolymers* **2006**, *84*, 519−526.
(43) Auer, S.; Trovato, A.; Vendruscolo, M. *PLoS Comput. Biol.* **2009**, *5*, e1000458.
(44) Morriss-Andrews, A.; Bellesia, G.; Shea, J.-E. *J. Chem. Phys.* **2011**, *135*, 085102.
(45) Morriss-Andrews, A.; Shea, J.-E. *J. Chem. Phys.* **2012**, *136*, 065103.
(46) Yu, X.; Wang, Q.; Lin, Y.; Zhao, J.; Zhao, C.; Zheng, J. *Langmuir* **2012**, *28*, 6595−6605.
(47) Wadhwani, P.; Strandberg, E.; Heidenreich, N.; Bürck, J.; Fanghänel, S.; Ulrich, A. S. *J. Am. Chem. Soc.* **2012**, *134*, 6512−6515.
(48) Campioni, S.; Carret, G.; Jordens, S.; Nicoud, L.; Mezzenga, R.; Riek, R. *J. Am. Chem. Soc.* **2014**, *136*, 2866−2875.
(49) Shen, L.; Adachi, T.; Vanden Bout, D.; Zhu, X.-Y. *J. Am. Chem. Soc.* **2012**, *134*, 14172−14178.
(50) Losic, D.; Martin, L. L.; Aguilar, M.-I.; Small, D. H. *Biopolymers* **2006**, *84*, 519−26.